

# Development and evaluation of a self-assembled nanoparticle-based prodrug for sustained delivery of 4-phenylbutyric acid

Kikka Maeda<sup>a,\*</sup>, Babita Shashni<sup>a,b,\*</sup>, Hirofumi Matsui<sup>c</sup> and Yukio Nagasaki<sup>a,d,e,f,g</sup>

<sup>a</sup>Department of Materials Science, Graduate School of Pure and Applied Sciences, University of Tsukuba, Ibaraki, Japan;

<sup>b</sup>Organization for Research and Development of Innovative Science and Technology, Kansai University, Osaka, Japan;

<sup>c</sup>Division of Gastroenterology, Faculty of Medicine, University of Tsukuba, Ibaraki, Japan;

<sup>d</sup>Master's School of Medical Sciences, Graduate School of Comprehensive Human Sciences, University of Tsukuba, Ibaraki, Japan;

<sup>e</sup>Center for Research in Isotopes and Environmental Dynamics (CRIED), University of Tsukuba, Ibaraki, Japan;

<sup>f</sup>Department of Chemistry, Graduate School of Science, The University of Tokyo, Tokyo, Japan;

<sup>g</sup>High-value Biomaterials Research and Commercialization Center (HBRCC), National Taipei University of Technology, Taipei, Taiwan

## ABSTRACT

4-Phenylbutyric acid (PBA) is a small molecule with promising therapeutic potential for treating various diseases, including cancer and neurodegenerative disorders, due to its dual ability to reduce endoplasmic reticulum stress and inhibit histone deacetylases. However, its clinical application is hindered by rapid clearance from the body, necessitating frequent dosing that increases the risk of adverse effects. To address these limitations, we developed a nanoparticle-based prodrug (Nano<sup>PBA</sup>) utilizing the amphiphilic block copolymer poly(ethylene glycol)-*b*-poly(vinyl 4-phenylbutyrate) [PEG-*b*-P(VPBA)]. This system self-assembles into micelles, enabling controlled and sustained PBA delivery. The synthesis and characterization of Nano<sup>PBA</sup> revealed its high stability under physiological conditions and enzyme-responsive PBA release. Nano<sup>PBA</sup> demonstrated a controlled release profile *in vitro*, reducing burst release while maintaining therapeutic efficacy. Cytotoxicity assays using normal cell lines, including endothelial cells (BAEC), macrophages (RAW264.7), and rat gastric cells (RGM-1), showed minimal cytotoxic effects compared to the parent low-molecular-weight PBA. Furthermore, *in vivo* studies conducted in healthy C57BL/6J mice confirmed Nano<sup>PBA</sup>'s biocompatibility, with no significant adverse effects observed at therapeutic doses ranging from 200 to 500 mg-PBA/kg via oral administration. In conclusion, Nano<sup>PBA</sup> offers a controlled release profile, enhanced biocompatibility, and reduced toxicity, addressing the limitations associated with conventional PBA administration. These attributes make Nano<sup>PBA</sup> a promising candidate for improving the therapeutic efficacy and safety of PBA in clinical applications, particularly in diseases where maintaining consistent drug levels is crucial for treatment outcomes.

## ARTICLE HISTORY

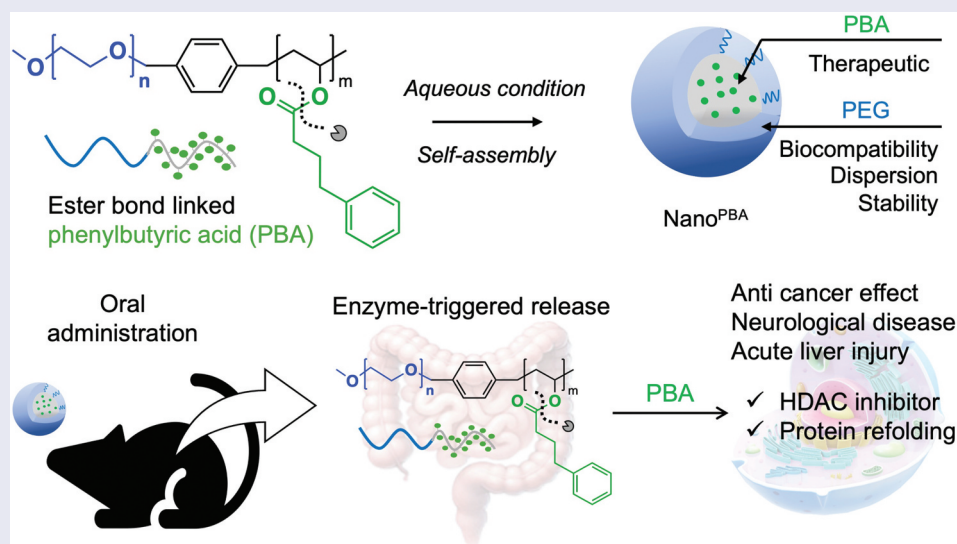
Received 23 December 2024

Revised 2 March 2025

Accepted 17 March 2025



## KEYWORDS

4-phenylbutyric acid;  
endoplasmic reticulum stress  
modulation; amphiphilic  
block copolymer micelle;  
chemical chaperone;  
prodrug of short chain fatty  
acid; sustained drug release



## IMPACT STATEMENT

We developed a self-assembled nanoparticle-based prodrug (Nano<sup>PBA</sup>) using an amphiphilic block copolymer for controlled 4-phenylbutyric acid (PBA) delivery, enabling enzyme-triggered release and improved therapeutic efficacy.

**CONTACT** Yukio Nagasaki  [nagasaki@ims.tsukuba.ac.jp](mailto:nagasaki@ims.tsukuba.ac.jp)  Department of Materials Science, Graduate School of Pure and Applied Sciences, University of Tsukuba, Ibaraki 305-8573, Japan

\*Equal contribution.

© 2025 The Author(s). Published by National Institute for Materials Science in partnership with Taylor & Francis Group.

This is an Open Access article distributed under the terms of the Creative Commons Attribution-NonCommercial License (<http://creativecommons.org/licenses/by-nc/4.0/>), which permits unrestricted non-commercial use, distribution, and reproduction in any medium, provided the original work is properly cited. The terms on which this article has been published allow the posting of the Accepted Manuscript in a repository by the author(s) or with their consent.

## 1. Introduction

Endoplasmic reticulum (ER) stress arises when the influx of proteins into the ER exceeds the capacity to process them, often due to factors such as protein misfolding or reduced calcium levels in the ER [1,2]. In response, cells activate the unfolded protein response (UPR), which aims to restore ER function by halting protein translation, degrading misfolded proteins, and simultaneously increasing molecular chaperones to aid proper protein folding. If these objectives are not achieved, the UPR can lead to apoptosis [1–3].

ER stress represents a key role in cancer development by interacting with oncogenic signalling pathways, upregulating survival pathways, angiogenesis, and metastasis [4]. It also contributes to chemoresistance, reducing the effectiveness of conventional cancer therapies [4], and modulates the immune response, enabling immune evasion by tumors [5]. Targeting ER stress pathways, particularly to activate the UPR and induce cancer cell death, are being explored as a potential cancer treatment, with compounds like Tamoxifen, Faslodex, trimethylamine N-oxide, and 4-phenylbutyric acid (PBA) under investigation [6–9].

PBA, an aromatic short-chain fatty acid (SCFA), is Food and Drug Administration (FDA) approved for treating urea cycle disorder by scavenging ammonia and aiding detoxification [10]. It also inhibits histone deacetylases (HDACs), leading to gene expression changes that can induce cell cycle arrest, apoptosis, and differentiation – key processes in cancer treatment [11]. PBA functions as a low-molecular-weight (LMW) chemical chaperone, aiding the refolding of misfolded proteins and reducing the endoplasmic reticulum (ER) stress, which may benefit neurodegenerative diseases like Alzheimer's [12,13]. Although the precise mechanism is not fully understood, it is believed that PBA interacts with the hydrophobic

regions of misfolded proteins, preventing aggregation and reducing the accumulation of misfolded proteins [14].

Despite promising anti-cancer effects of PBA *in vitro* [11,15], reports on its *in vivo* efficacy are scarce due to poor pharmacokinetics, including rapid initial increase in blood drug concentration followed by a sharp decrease and fast clearance and rapid metabolism and clearance from the body following administration [16]. The brief half-life of PBA is approximately 45 min, renders it challenging to sustain its inhibitory effect on ER stress in the liver tissue over an extended period [16]. Consequently, frequent administration of the drug is necessary to maintain the desired effect, leading to adverse effects such as taste disorders, gastrointestinal disturbances, and menstrual insufficiency [17]. The mitigation of these complications via improving pharmacokinetic characteristics is a crucial aspect of the prospective utilization of PBA as a therapeutic agent.

SCFAs like propionic acid and butyric acid are therapeutically effective but have poor pharmacokinetic properties. To address this, we have incorporated SCFAs into amphiphilic block copolymers as prodrugs, which self-assemble into polymeric micelle-type nanoparticles, enhancing their therapeutic efficacy (Figure 1) [18–21]. These micelles are comprised of an amphiphilic block copolymer, poly(ethylene glycol)-*b*-poly(vinyl SCFA), which self-assembles into tens of nanometer-sized micelles (Nano<sup>SCFA</sup>) under aqueous conditions [18–21]. Our previous research has shown that polymeric micelles constructed from amphiphilic block copolymers remain stable even at low concentrations despite being self-organized molecular assemblies. This stability is attributed to the entanglement of hydrophobic chains in the core and the dense polyethylene glycol (PEG) brush forming the shell, which

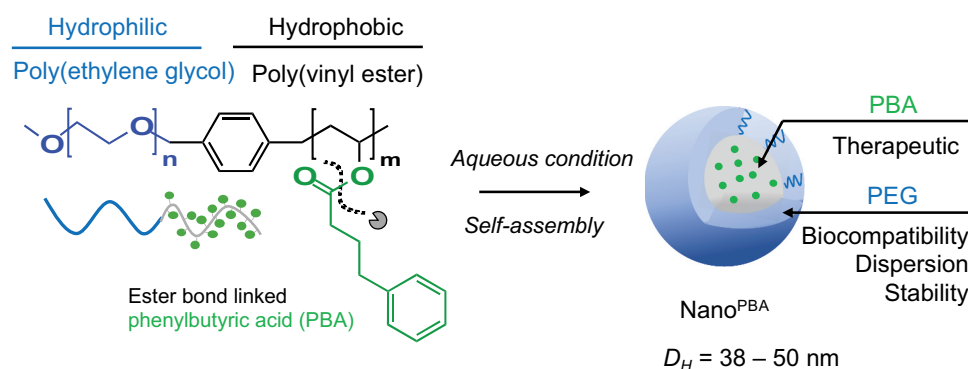


**Figure 1.** Design of self-assembling block copolymer-based 4-phenylbutyric acid prodrug (Nano<sup>PBA</sup>). Poly(ethylene glycol)-*b*-poly(vinyl phenylbutyrate) (PEG-*b*-P(VPBA)) is composed of hydrophilic PEG and hydrophobic poly(vinyl phenylbutyrate), which self-assembles into polymeric micelle under aqueous condition with 38–50 nm of hydrodynamic diameter [18–21]. Several dozens of units of 4-phenylbutyric acids are conjugated to the main polymer chain through enzyme-cleavable ester linkage [18–21].

suppresses particle aggregation and protein adsorption, enabling effective dispersion even under harsh *in vivo* conditions [18–21]. As a result, these micelles exhibit significantly higher accumulation in the intestinal mucosa compared to commercially available polystyrene nanoparticles when administered orally. Once in the intestinal mucosa, these self-assembled polymeric micelles gradually disintegrate under high viscosity and protein-rich conditions, exposing the encapsulated SCFA esters in the core and allowing them to undergo enzymatic hydrolysis. Building on these findings, we have developed a PBA-based self-assembled prodrug (Nano<sup>PBA</sup>) consisting of an amphiphilic block copolymer, poly(ethylene glycol)-*b*-poly(vinyl phenylbutyrate) (PEG-*b*-P(VPBA)) to overcome its drawbacks of PBA. Nano<sup>PBA</sup> is anticipated that LMW PBAs conjugated to the hydrophobic segment of the polymer via an ester linkage will be hydrolytically liberated by physiological esterase, thereby enhancing their pharmacokinetic properties such as controlled and sustained release for an extended period (Figure 1) [18–21]. The objective of this study is to synthesize PEG-*b*-P(VPBA) with different PBA units, prepare their respective Nano<sup>PBA</sup>, their *in vitro* characterization such as critical micelle concentration (CMC), stability studies, PBA release profile, and dose-dependent safety studies in a healthy C57/BL6 mice in comparison with LMW PBA.

## 2. Materials and methods

### 2.1. Materials and reagents

All the chemicals used for the synthesis were purchased from Sigma-Aldrich (Japan), Tokyo Kasei Kogyo Co. (Japan), and Fujifilm Wako Pure Chemical (Japan) and were used as received [18–26].

### 2.2. Synthesis of MeO-PEG-CH<sub>2</sub>PhCH<sub>2</sub>Cl

The synthesis of MeO-PEG-CH<sub>2</sub>PhCH<sub>2</sub>Cl was performed following a previously reported method with some modifications (Figure 2) [18–20]. Briefly, the benzyl chloride group was introduced at the end of MeO-PEG-OH. Fifty grams of MeO-PEG-OH (5 k) were dried in a flask under vacuum at 110°C for 12 h. Afterward, 100 mL of super-dehydrated tetrahydrofuran (THF) was added under a nitrogen atmosphere, followed by 13 mL of butyllithium (BuLi, 1.6 M in hexane, 20 mmol) to convert the hydroxyl end groups of MeO-PEG-OH into lithium alkoxide at a 1:2 molar ratio. Seventeen grams of  $\alpha,\alpha$ -dichloro-*p*-xylene (100 mmol) was then added to the solution and stirred at 50°C for 48 h. Once the reaction was complete, the polymer solution was precipitated in isopropyl alcohol (IPA) at –30°C and centrifuged at 15,000  $\times$  g for

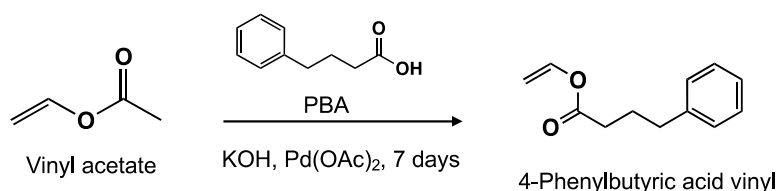
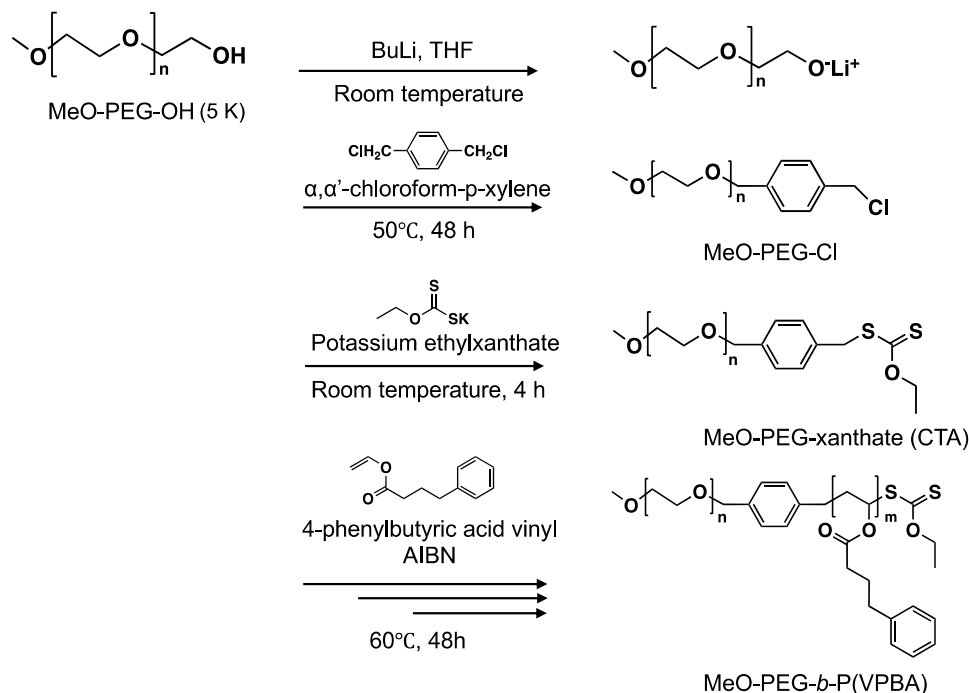
15 min at –4°C. The precipitated polymer was dissolved in methanol and re-precipitated in cold IPA. This process was repeated three times to remove unreacted  $\alpha,\alpha$ -dichloro-*p*-xylene and to purify the MeO-PEG-CH<sub>2</sub>PhCH<sub>2</sub>Cl polymer. The purified polymer was vacuum-dried at room temperature (around 25°C) for 12 h to eliminate any residual IPA. Finally, the polymer was characterized using proton nuclear magnetic resonance (<sup>1</sup>H-NMR, JEOL 400 MHz) and gel permeation chromatography (GPC, JASCO Co. Ltd. CO-2060Plus, column: TSKgel-GMH-M) with THF as the eluent.

### 2.3. Synthesis of MeO-PEG-Xanthate (CTA)

MeO-PEG-xanthate was synthesized as a chain transfer agent for reversible addition-fragmentation transfer (RAFT) polymerization with minor modifications to previous methods (Figure 2) [18–21] as follows; 5 g of MeO-PEG-CH<sub>2</sub>PhCH<sub>2</sub>Cl was dissolved in 50 mL methanol under N<sub>2</sub> atmosphere, followed by the addition of 0.21 g of potassium ethylxanthate and stirred at room temperature for 4 h. After the reaction, the solution was filtered with filter paper (pore size: 7  $\mu$ m, thickness: 0.22 mm) and Celite (FUJIFILM Wako Pure Chemical) to remove the impurities. The filtered solution was precipitated in IPA at –30°C and centrifuged at 15,000  $\times$  g for 15 min at –4°C. The precipitated polymer was dissolved in methanol and re-precipitated in cold IPA. This process was repeated three times to remove the unreacted potassium ethylxanthate and purify the MeO-PEG-xanthate. The polymer was then vacuum-dried for 12 h to remove any residual solvent. The chemical structure of the obtained polymer was analysed by <sup>1</sup>H-NMR and GPC in THF as eluent.

### 2.4. Synthesis of 4-phenylbutyric acid vinyl (vinyl 4-phenylbutyrate)

Vinyl 4-phenylbutyrate (VPBA) as a monomer for RAFT polymerization was synthesized by a transvinylation reaction (Figure 2) [27]. Sixty grams of PBA, 17.5 mg of palladium(II) acetate (Pd(OAc)<sub>2</sub>), and 70 mg of potassium hydroxide were added in a flask under an N<sub>2</sub> atmosphere. Then, 75 mL of vinyl acetate was added and stirred at room temperature for 72 h. After the reaction, the solution was filtered through Celite to remove Pd(OAc)<sub>2</sub>, and then the unreacted vinyl acetate and acetic acid were removed using a rotary evaporator. The same amount of Pd(OAc)<sub>2</sub>, potassium hydroxide, and vinyl acetate were then added to the resulted solution and reacted again at room temperature for another 72 h. After the reaction, impurities were removed in the same manner as described above. The pure vinyl

**(a) Synthesis scheme of 4-phenylbutyric acid vinyl (PBA)****(b) Synthesis scheme of PEG-*b*-P(VPBA)**

**Figure 2.** (a) Synthesis scheme of 4-phenylbutyric acid vinyl. (b) Synthesis scheme of PEG-*b*-P(VPBA) block copolymer by RAFT polymerization.

4-phenylbutyrate was purified by distillation at 80°C under 20 Pa (boiling point: 273 °C). The structure of the obtained compound was analysed by <sup>1</sup>H-NMR.

## 2.5. Synthesis of MeO-PEG-*b*-P(VPBA)

The amphiphilic block copolymer, MeO-PEG-*b*-P (VPBA), was synthesized by RAFT polymerization of VPBA in the presence of MeO-PEG-xanthate (Figure 2) [17–19]. The synthesized MeO-PEG-xanthate, VPBA, and 2,2'-azobis(isobutyronitrile) (AIBN) were mixed in a flask. The nitrogen gas was bubbled through the solution for 10 min to remove oxygen and the reaction was carried out at 60°C in an oil bath for 48 h. After the reaction, 50 mL of tetrahydrofuran (THF) was added to dissolve the reaction mixture completely. The solution was then added to 1000 mL of IPA at –30°C, and the polymer precipitate was collected by centrifugation (15,000 rpm, 2000 × g, 15 min). The supernatant IPA was then discarded, and the precipitate was completely dissolved by heating at 60°C. The polymer was precipitated with cold IPA and

centrifuged again. This process was repeated thrice. Finally, the polymer was dried under reduced pressure at room temperature. The chemical structure and the molecular weight and the distribution of the obtained polymers were analysed by <sup>1</sup>H NMR and GPC in THF eluent. The block copolymer with different degrees of polymerization was prepared by changing the molar ratio of VPBA to MeO-PEG-xanthate.

## 2.6. Preparation of 4-phenylbutyric acid nanoparticles (Nano<sup>PBA</sup>) and stability studies

4-Phenylbutyrate-installed nanoparticles (Nano<sup>PBA</sup>) were prepared via self-assembly of amphiphilic block copolymer MeO-PEG-*b*-P(VPBA) under aqueous conditions [17–19]. One hundred milligrams of the block copolymer was dissolved in 1 mL of N,N-dimethylformamide (DMF) and was dialyzed against deionized water (2 L, 1/2000, v/v) using a semipermeable membrane (MWCO = 3.5 kDa, Spectra/Por®, U.S.A.) for 3–4 days, with the dialysate changed every 12 h. The



size of the resulting micelles was measured by dynamic light scattering (DLS) using a Zetasizer Nano ZS (Malvern, UK).

The effect of polymer concentration on micelle formation at room temperature was evaluated using DLS, as previously described [20,28]. CMC of Nano<sup>PBA</sup> was determined using a fluorescent probe method with pyrene (Sigma-Aldrich). Briefly,  $6 \times 10^{-5}$  M pyrene solution in acetone (10  $\mu$ L) was added to 1.5 mL vials and allowed the acetone to evaporate completely by incubating at 30°C for 30 min. Various concentrations of Nano<sup>PBA</sup> polymer solution (1 mL) were then added to the vial containing pyrene to achieve a final pyrene concentration of  $6 \times 10^{-7}$  M. The samples were equilibrated overnight at room temperature (25°C) with agitation at 100 rpm. Pyrene fluorescence excitation spectra were measured with an emission wavelength ( $\lambda_{em}$ ) of 370 nm using a fluorescence spectrophotometer (F-7000, FL Solutions 4.2, Hitachi High-Tech, Japan).

The stability of the micelles over a pH range of 1–13 was evaluated by dynamic light scattering (DLS) measurements. A 0.5 mL aliquot of the prepared Nano<sup>PBA</sup> solution (10 mg polymer/mL) was mixed with 2.5 mL of hydrochloric acid (0.1 M) or sodium hydroxide solution (0.1 M), and the pH was adjusted with gentle stirring. The size distribution and polydispersity index (PDI) of the Nano<sup>PBA</sup> solution were then monitored by calculation of scattering intensity over a predetermined time frame (0–48 h) to assess its stability as a function of pH.

To evaluate the time-dependent stability of the micelles in a sodium chloride (NaCl) solution, and NaCl solution (300 mM, Milli-Q water) was mixed with the Nano<sup>PBA</sup> solution (10 mg-polymer/mL) in a 1:1 ratio (final concentration is 150 mM). The samples were incubated at 37°C with gentle shaking at 100 rpm. The size distribution and PDI were measured at various time intervals (0–48 h) by calculation of scattering intensity using DLS.

The stability of micelles under digestive conditions was evaluated using fed-state simulated intestinal fluid (SIF, Biorelevant) and fed-state simulated colonic fluid (SCF, Biorelevant). Nano<sup>PBA</sup> (20  $\mu$ g PBA/mL) was mixed with SIF or SCF in a 1 : 1 ratio, resulting in a final concentration of 10  $\mu$ g PBA/mL. The samples were incubated at 37°C with gentle shaking at 100 rpm. Size distribution were measured at various time intervals (0–48 h) by analyzing scattering intensity using DLS.

## 2.7. In vitro release profile of PBA from Nano<sup>PBA</sup>

An *in vitro* release profile was conducted to validate the enzyme-responsive release of PBA from Nano<sup>PBA</sup> [18–20]. Nano<sup>PBA</sup> (10  $\mu$ g PBA/mL) was mixed with esterase (40 U/mL) in 1 mL of phosphate-buffered

saline (PBS), and simulated digestive fluids (SIF and SCF) (Biorelevant) over a period of 0–48 h. The release of PBA was monitored using a Liquid Chromatography/Mass Spectrometry (LC-MS/MS) system, which included a HITACHI LaChrom ULTRA liquid chromatograph coupled with an AB Sciex API 2000 mass spectrometer. An ODS-100Z TSK-gel (3  $\mu$ m) column was used for separation of the targeted peaks. The mobile phase, comprising acetonitrile (ACN) and water (H<sub>2</sub>O) in a 1:1 ratio with 0.1% formic acid (FA), was employed as the running solvent for liquid chromatography (LC). The total ion chromatogram (TIC) was used to evaluate the mass spectra of the precursor and fragment ions. The mass-to-charge ratio ( $m/z$ ) of the precursor ion of PBA was detected as 162.9 Da under the following MS conditions: negative mode, delustering potential of –24, focusing potential of –320, entrance potential of –10, and ion spray voltage of –4500 V. A characteristic fragment ion with an  $m/z$  of 91.2 Da was identified from the precursor ion. The samples were centrifuged at 15,000  $\times$  rpm for 30 min at 4°C, and the supernatants were diluted with 50% ACN containing 0.1% FA. Fifty microliters of each sample were injected into the LC-MS/MS system, with a flow rate of 0.2 mL/min. The liberated PBA was quantified using a calibration curve prepared with several authentic PBA solutions in PBS, SIF, and SCF.

## 2.8. Cytotoxicity of Nano<sup>PBA</sup>

Viability assays were performed according to the manufacturer's instructions (Cell Counting Kit-8, Dojindo Laboratories) [20]. The macrophage cell line (RAW264.7), bovine aortic endothelial cell line (BAEC), and rat gastric epithelial cell line (RGM-1) were seeded at a density of 7,000 cells per well in 96-well plates. Following overnight incubation, the cells were exposed to several equimolar concentrations of Nano<sup>PBA</sup> and LMW PBA. After 24 h, the cells were washed with warm PBS (twice) to remove any traces of samples and incubated further for 2 h with 2-(2-methoxy-4-nitrophenyl)-3-(4-nitrophenyl)-5-(2,4-disulfo-phenyl)-2-h-tetrazolium, monosodium salt (WST-8) diluted in fresh medium (100  $\mu$ m). The amount of formazan formed was measured at 450 nm, with background correction at 600 nm, using a microplate reader (Thermo SCIENTIFIC VARIOSKAN FLASH, Type 3001). The final optical density values were expressed as a percentage of the untreated control.

## 2.9. In vivo toxicity

The animal studies in this work were conducted according to the guidelines of the Institutional Animal Care and Use Committee at the University of Tsukuba (approval no. 23–309) [19–

21,27]. The mice were housed in a pathogen-free environment with controlled conditions, including  $52.5 \pm 12.5\%$  humidity,  $23.5 \pm 2.5^\circ\text{C}$  temperature, and a lighting schedule from 5:00 to 19:00. They had free access to standard chow diet. The mice were acclimated for one week before experiments began. Male C57BL/6J mice, obtained from the Jackson Laboratory (Japan), were used for the studies.

After a one-week acclimation period, male C57BL/6 mice (5 weeks of age) were randomly assigned to 13 groups ( $n = 3$ ), including a healthy control group (water only), three groups treated with PBA at doses of 100, 200, and 500 mg/kg body weight (BW), and nine groups treated with Nano<sup>PBA</sup> at the same PBA doses, but with three types of degrees of polymerization ( $m = 9, 30, 49$ ) (100, 200, and 500 mg-PBA/kg BW). The sample solutions were administered orally in a single dose, and the mice were observed for 14 days. The changes in discomfort, food intake, sample consumption, and body weight were monitored. Following a 14-day observation period, the mice were euthanized under anesthesia, and blood and plasma samples were collected. Hematological parameters, including red blood cells, white blood cells, hemoglobin, and platelets, were quantified using a blood cell counter (Celltac  $\alpha$ , Nihon Kohden, Japan). Serum biochemical analysis was performed, including alanine transaminase (ALT), aspartate aminotransferase (AST), creatinine (CRE), blood urea nitrogen (BUN), albumin (ALB), creatine phosphokinase (CPK), and lactate dehydrogenase (LDH), using an automatic biochemical analyser (FUJI DRI-CHEM 7000 V, FUJIFILM, Japan). Additionally, the weights of the liver, spleen, and kidneys were measured to assess any potential toxicity resulting from the treatments.

## 2.10. Statistical analysis

The statistical analyses between the groups were performed using GraphPad Prism software version 9 (GraphPad Software Inc., San Diego, CA, U.S.A.). One-way ANOVA was employed to substantiate the statistical disparity between the groups. A  $p$ -value of less than 0.05 was considered statistically significant, indicating a meaningful difference between the groups.

## 3. Results

### 3.1. Synthesis of MeO-PEG-*b*-P(VPBA)

The amphiphilic block copolymer, MeO-PEG-*b*-P(VPBA), was synthesized by reversible addition-

fragmentation chain transfer (RAFT) polymerization (Figure 2) [19–21,27]. The vinyl 4-phenylbutyrate (VPBA) was prepared via a transvinylolation reaction (Figure 2a). A PEG-based chain transfer agent, MeO-PEG-xanthate, was synthesized according to our previous articles [19–21,27]. RAFT polymerization of VPBA was carried out in the presence of MeO-PEG-xanthate, initiated with AIBN as the radical initiator, resulting in the formation of MeO-PEG-*b*-P(VPBA) (Figure 2b). The molar ratio of VPBA to MeO-PEG-xanthate was varied using PEG with a molecular weight of 5 kDa, to obtain polymers with different compositions. The hydrophobic poly(vinyl phenylbutyrate) (P(VPBA)) segments in the block copolymer consist of tens of PBA units, which are introduced as side chains via ester bonds (Figures 1 and 3a). As shown in the  $^1\text{H}$ -NMR spectrum (Figure 3b–d), approximately 9, 30, and 49 PBA units were introduced to the polymer backbone.

The GPC traces of PEG-*b*-P(VPBA) showed higher molecular weights for all samples ( $m = 9$ ,  $M_n = 5,600$ ,  $M_w/M_n = 1.44$ ;  $m = 30$ ,  $M_n = 6,959$ ,  $M_w/M_n = 1.61$ ;  $m = 49$ ,  $M_n = 8,501$ ,  $M_w/M_n = 1.70$ ) compared to commercial MeO-PEG-OH ( $M_n = 4,829$ ,  $M_w/M_n = 1.09$ ) and MeO-PEG-xanthate chain transfer agent ( $M_n = 5,130$ ,  $M_w/M_n = 1.20$ ) (Figure 3e–f). The presence of two peaks in the GPC measurements of PEG is attributable to the commercial methoxy-PEG-OH (Merck), which inherently contains two peaks. These results demonstrate the successful synthesis of PEG-*b*-P(VPBA) with varying PBA units.

### 3.2. Preparation of Nano<sup>PBA</sup> and its stability under physiological conditions

Nano<sup>PBA</sup>s were prepared by the self-assembly of amphiphilic PEG-*b*-P(VPBA) block copolymers in an aqueous solution. The PEG-*b*-P(VPBA) polymer, dissolved in DMF, was subjected to dialysis against dd water for several days using a semi-permeable membrane ( $MWCO = 3.5$  kDa), with the dialysate being changed twice daily. The ratio of polymer solution versus dialysate was 1/2000 mL. The hydrodynamic size ( $D_H$ ) of the obtained micelles (Nano<sup>PBA</sup>) was determined by DLS. The intensity and volume distributions of Nano<sup>PBA</sup> revealed that the hydrodynamic diameter varied with the number of PBA units in the poly(vinyl ester) segments ( $m = 9$ ,  $38.3 \pm 0.72$  nm,  $22.2 \pm 6.59$  nm;  $m = 30$ ,  $40.8 \pm 0.25$  nm,  $29.7 \pm 1.47$  nm;  $m = 49$ ,  $50.4 \pm 0.28$  nm,  $42.8 \pm 0.85$  nm) with a narrow polydispersity index (PDI) ( $m = 9$ ,  $0.25 \pm 0.02$ ;  $m = 30$ ,  $0.14 \pm 0.01$ ;  $m = 49$ ,  $0.09 \pm 0.01$ ) and autocorrelation curve with minimal fluctuation at room temperature, indicating uniformity in the micelle size (Figure 4a–c, Table 1).

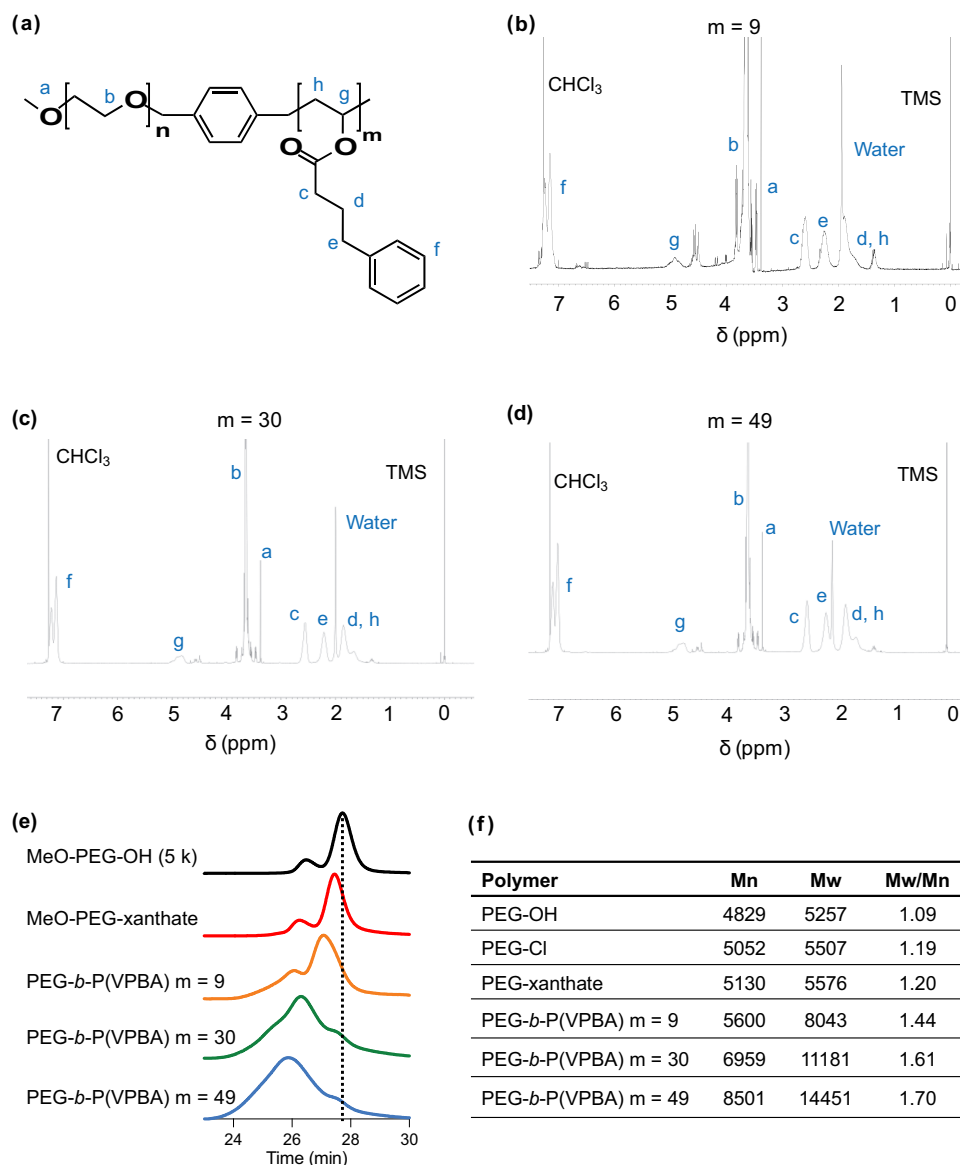


**Figure 3.** Analysis of the synthesized polymer by  $^1\text{H-NMR}$  and GPC. (a) Structure of PEG-*b*-P(VPBA).  $^1\text{H-NMR}$  spectrum of (b)  $m = 9$ , (c)  $m = 30$ , and (d)  $m = 49$  units of the block copolymer. The degree of polymerization (DP) was calculated by integral value. (e) The GPC curves of the polymers. (f) Calculated molecular weight of the polymers by GPC.

Following successful micelle preparation, we evaluated the stability of Nano<sup>PBA</sup> under various pH conditions to check its suitability for oral administration. The stability of Nano<sup>PBA</sup> was assessed by the DLS parameters. As shown in Figure 4d–f, at acidic and neutral pH conditions (pH = 1–9), the PDI for each micelle remained constant at all time points up to 48 h, while under the strong alkaline conditions (pH = 10–13), an increase in the PDI value was observed after 48 h. These data suggest that under the conditions investigated, Nano<sup>PBA</sup> is expected to maintain micelle structure in the stomach, making it suitable for oral administration. Some of the ester groups in the copolymer may have been hydrolyzed under strong alkaline conditions, leading to an increase in the PDI over 48 h. The time-dependent stability of Nano<sup>PBA</sup> (10 mg – polymer/mL) was then evaluated in a physiological NaCl solution (150 mM, Milli Q water). As shown in Figure 4g–i,

Nano<sup>PBA</sup> maintained its structural integrity in 150 mM NaCl, as evidenced by negligible changes in the hydrodynamic diameter for at least 48 h. On the other hand, the size of Nano<sup>PBA</sup> (10 mg polymer/mL) in simulated digestive fluids (SIF, SCF) gradually increased over time, as shown in Figure 4j–o. This increase is likely due to the enzymatic and ionic activity in the intestine, which facilitates micelle disintegration and promotes aggregation by exposing hydrophobic segments.

The impact of polymer concentration on nanoparticle formation was evaluated by DLS. The CMC of Nano<sup>PBA</sup> was determined using pyrene as a fluorescent probe, following previously described methods [20,28]. Pyrene's photophysical behavior reflects its localization in either the hydrophobic core of a micelle or a hydrophilic environment. The characteristic vibrational band of pyrene ( $6 \times 10^{-7}$  M) at an

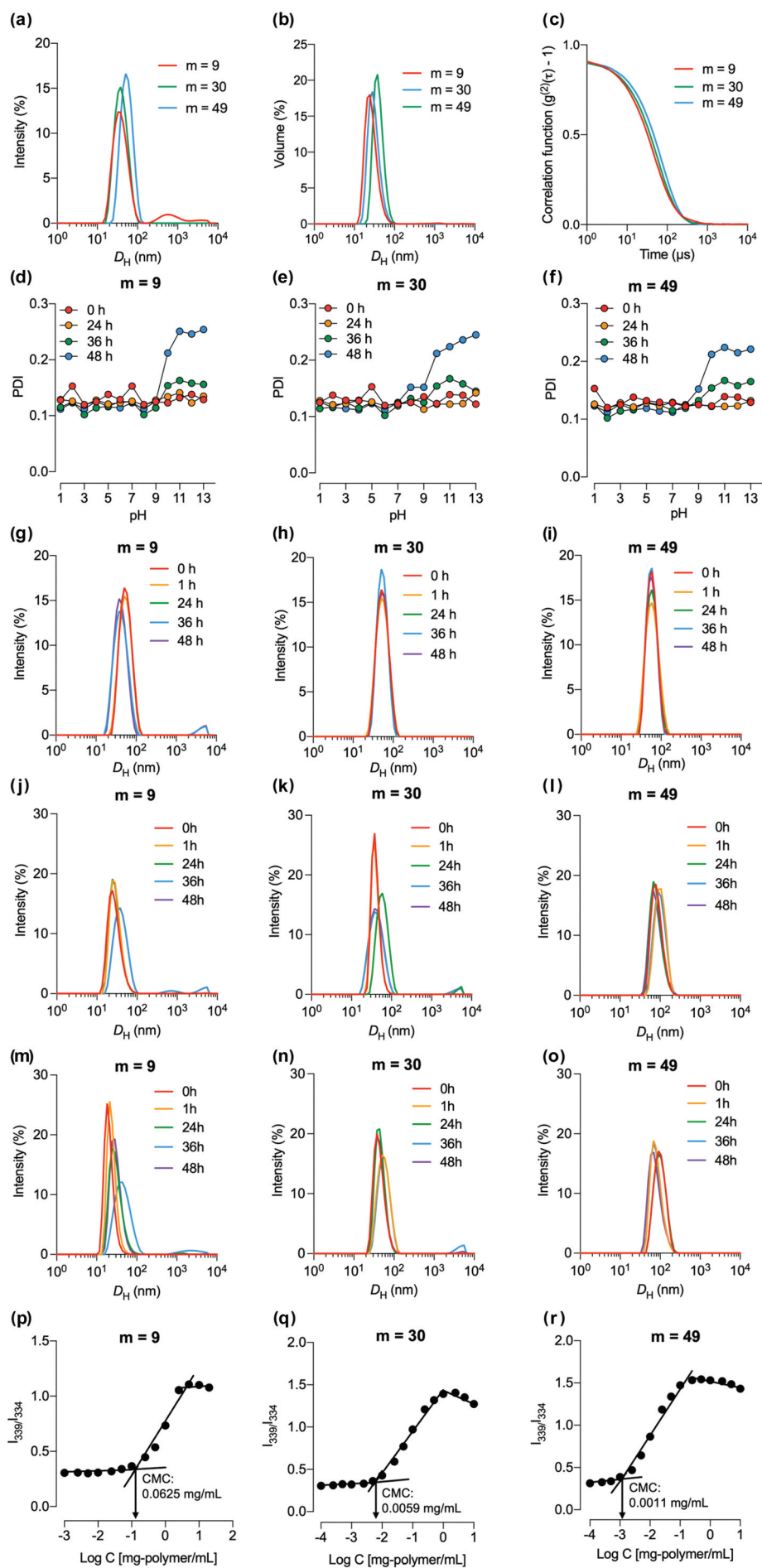


**Figure 4.** Characterization of Nano<sup>PBA</sup>. (a) The intensity and (b) volume-based size distribution, and (c) auto correlation function of Nano<sup>PBA</sup> (20 mg-polymer/mL) determined by DLS. The respective PDI of Nano<sup>PBA</sup> (10 mg-polymer/mL) under several pH at 37°C



**Table 1.** Properties of Nano<sup>PBA</sup> for each formulation. Size, PDI, and CMC for each formulation of the micelle were indicated.

Nano <sup>PBA</sup>	Size (Intensity, nm)	Size (Volume, nm)	PDI	CMC (mg/L)
m = 9	38.3 ± 0.72	22.2 ± 6.59	0.25 ± 0.02	62.5
m = 30	40.8 ± 0.25	29.7 ± 1.47	0.14 ± 0.01	5.9
m = 49	50.4 ± 0.28	42.8 ± 0.85	0.09 ± 0.01	1.1

emission wavelength of  $\lambda_{em} = 370$  nm shifts from  $I_{334}$  (pyrene in water) to  $I_{339}$  (pyrene within the hydrophobic core of the micelle). The ratio of  $I_{339}$  to  $I_{334}$  serves as an indicator of micelle formation. As shown in Figure 4p–r, the data exhibited a sigmoidal response in the  $I_{339}/I_{334}$  ratio when plotted against the logarithm of the PEG-*b*-P(VPBA) concentration. The CMC values were determined based on the inflection points in the sigmoidal emission curves and were found to be approximately 62.5 mg/L (for  $m = 9$ ), 5.9 mg/L (for  $m = 30$ ), and 1.1 mg/L (for  $m = 49$ ) for PEG-*b*-P(VPBA). The obtained data demonstrate that increasing the length of the hydrophobic chain of PEG-*b*-P(VPBA) reduces the CMC values, indicating that micelles with longer hydrophobic chains have enhanced stability. The results suggest that the nanostructure of Nano<sup>PBA</sup> demonstrates prolonged stability in diluted biological fluids. This enhanced stability is due to the thermodynamically controlled disintegration process of the polymeric micelles, where the equilibrium between micelle formation and dissociation governs their structural stability over an extended duration.

### 3.3. Enzyme-responsive PBA release from Nano<sup>PBA</sup>

An *in vitro* release profile was determined to confirm the enzyme-responsive PBA release from Nano<sup>PBA</sup> using an LC-MS/MS system. To optimize PBA detection, the mass spectra of the precursor ion (162.9 m/z) and fragment ion (91.2 m/z) were used (Figure 5a) [29]. A reliable calibration curve ( $R^2 = 0.994$ ) confirmed the suitability of the selected fragment ions for accurate PBA detection (Figure 5b–c). Nano<sup>PBA</sup> solution (10  $\mu$ g-PBA/mL PBS) was mixed with porcine liver esterase (40 U/mL) and incubated for a predetermined time (0–48 h), followed by detection using standardized LC-MS/MS conditions. As shown in Figure 5d–g, all Nano<sup>PBA</sup> groups showed evident time-dependent liberation of PBA in the presence of esterase compared with Nano<sup>PBA</sup> alone group,

indicating a successful hydrolysis of the ester linkage. In each formulation, PBA release exhibited a plateauing trend after 24 h. Key operational parameters influencing esterase activity include temperature, pH, substrate concentration, and enzyme concentration. As the enzymatic reaction progresses, PBA bound to the block polymer might gradually decrease, while its released concentration increases. This released PBA can modify the reaction environment by altering pH or interacting with the enzyme, potentially leading to enzyme inactivation and ultimately halting the hydrolysis process. The PBA liberation rate inversely correlated with the molecular weights of the hydrophobic segment in the block copolymers. Nano<sup>PBA</sup> with fewer PBA units, (i.e. shorter hydrophobic chain length) showed higher liberation:  $m = 9$  ( $55.2 \pm 5.9\%$ ) >  $m = 30$  ( $27.6 \pm 4.3\%$ ) >  $m = 49$  ( $17.7 \pm 0.7\%$ ) (Figure 5h). These results are corroborated by the area under the curve (AUC) values of the release profile graph (Figure 5i), which show that an increase in the hydrophobic segment length reduces the PBA release rate. Furthermore, the result of the release profile under SIF (Figure 5j–l), and SCF (Figure 5m–o) showed an enhanced release of PBA compared to the PBS condition. These results indicate that digestive conditions increase enzyme interactions and promote hydrolysis, leading to a higher release rate. This is likely due to shorter chain lengths in the P(VPBA) segment reducing hydrophobicity, which weakens the entanglement and core coagulation force within the hydrophobic core, thus accelerating core disintegration. Even short chains, such as  $m = 9$ , maintain sufficient stability under harsh conditions, including low pH and high ionic strength, typical of the gastrointestinal tract.

### 3.4. Cytotoxicity of Nano<sup>PBA</sup>

Cytotoxicity of Nano<sup>PBA</sup> was evaluated on several normal cell lines: BAEC (endothelial cell), RAW264.7 (macrophages), and gastric RGM-1 using WST-8 assay. After overnight cultivation, cells were treated with various

determined by DLS measurements: (d)  $m = 9$ , (e)  $m = 30$ , and (f)  $m = 49$ . Stability profiles of Nano<sup>PBA</sup> (10 mg-polymer/mL) confirmed by size in NaCl solution (150 mM): (g)  $m = 9$ , (h)  $m = 30$ , and (i)  $m = 49$ . The stability of Nano<sup>PBA</sup> (10 mg-polymer/mL) were conducted under physiological condition using SIF: (j)  $m = 9$ , (k)  $m = 30$ , (l)  $m = 49$ , and SCF: (m)  $m = 9$ , (n)  $m = 30$ , (o)  $m = 49$ . The critical micelle concentration (CMC) was determined by pyrene method [15]. Fluorescence intensity ratio  $I_{339}/I_{334}$  obtained from pyrene excitation spectra ( $\lambda_{em} = 370$  nm) in water ( $6 \times 10^{-7}$  M) in the presence of increasing concentration of PEG-*b*-P(VPBA) (mg- polymer/mL) of each unit (p)  $m = 9$ , (q)  $m = 30$ , and (r)  $m = 49$ .

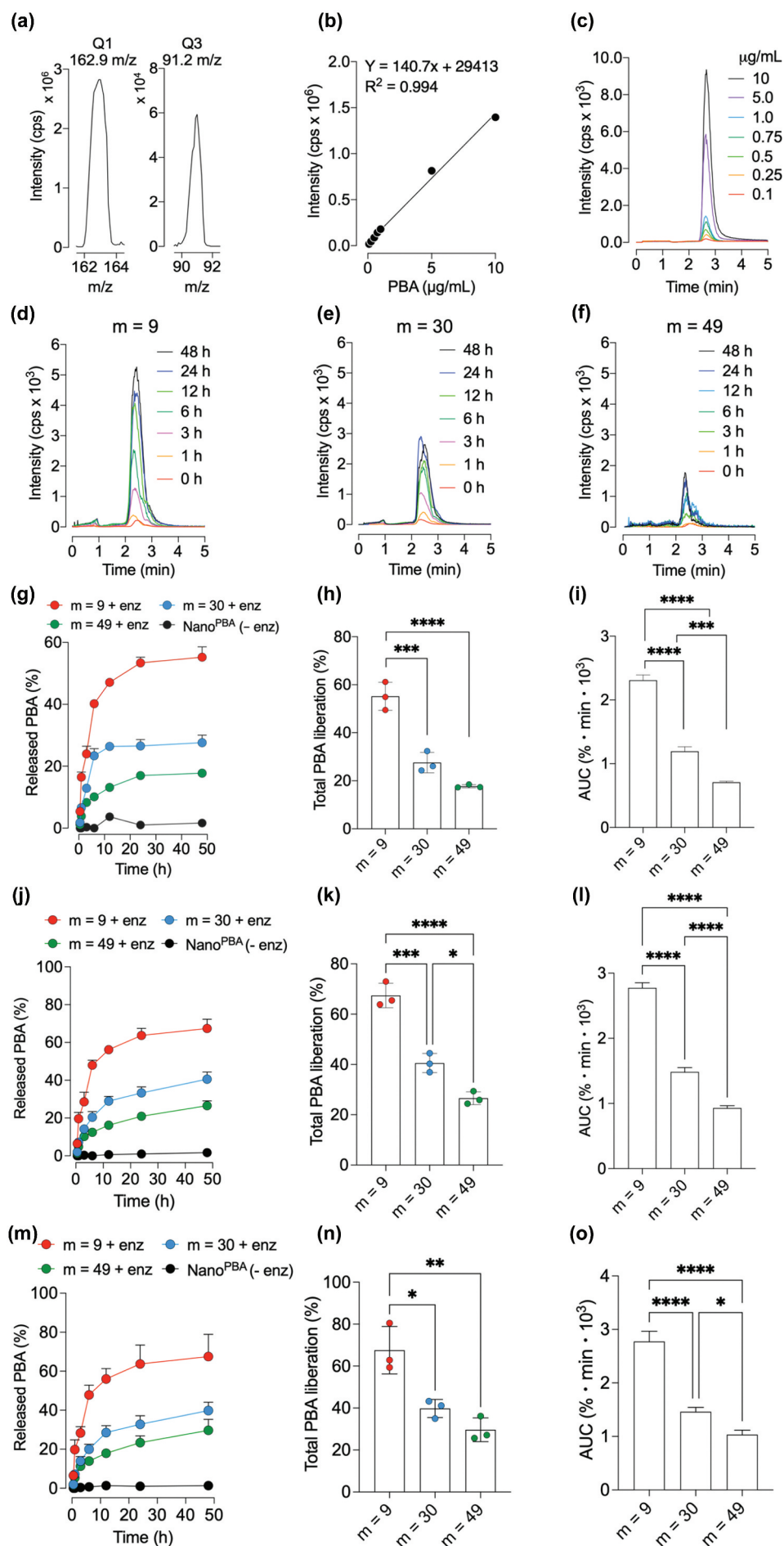


**Figure 5.** *In vitro* release profile of Nano<sup>PBA</sup> under esterase enzyme (enz). Nano<sup>PBA</sup> (10  $\mu\text{g}$ -PBA/mL) was digested with esterase (40 U/mL) in 1 mL of PBS for predetermined time (0–48 h). The PBA release was detected using an LC-MS/MS system. (a) Mass spectra

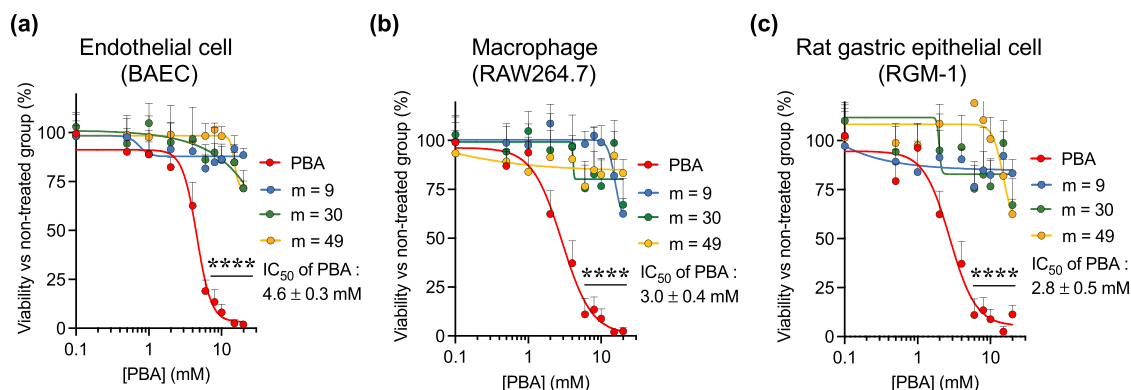


**Figure 6.** Cell viability studies of (a) bovine aortic endothelial cell (BAEC), (b) macrophage (RAW264.7), and (c) rat gastric epithelial cell (RGM-1) by cell counting kit-8 assay. Cytotoxicity assay examined at 24 h post-treatment. The data are presented as the means  $\pm$  S.E.M; \*\*\*\* $p < 0.0005$ , Dunnett's multiple comparisons test.

concentrations of Nano<sup>PBA</sup> and LMW PBA (0–20 mmol–PBA/L) for 24 h. In the PBA-treated group, a decrease in cell viability was observed with increasing concentration, with most cells exhibiting mortality at a concentration of 10 mM (Figure 6a–c). The 50% inhibitory concentration (IC<sub>50</sub>) of LMW PBA was determined to be  $4.6 \pm 0.3$  mM (BAEC),  $3.0 \pm 0.4$  mM (RAW264.7), and  $2.8 \pm 0.5$  mM (RGM-1). Conversely, the Nano<sup>PBA</sup>-treated group exhibited significantly high cell viability (non-detectable IC<sub>50</sub> value) at the same concentration of LMW PBA. No discernible difference in cell viability was observed between all Nano<sup>PBA</sup>-treated groups under the present conditions.

### 3.5. In vivo toxicity

We further investigated the toxicological changes upon Nano<sup>PBA</sup> and PBA administration *in vivo* by assessing parameters such as body and organ weights, plasma levels of organ damage markers, and hematology (Figure 7a). Healthy C57BL/6J mice were orally administered PBA and Nano<sup>PBA</sup> at equivalent doses (200, 500, and 1000 mg-PBA/kg-BW; 1.2, 3.0, and 6.0 mmol-PBA-/kg BW) and observed for 2 weeks. All treated groups showed a gradual increase in body weight, similar to the non-treated group, indicating no major toxicity (Figure 7b). Average food consumption/mouse/day (Figure 7c) also did not show any significant changes in all treated groups compared to the non-treated group. Kidney weight (Figure 7d) and spleen weight (Figure 7e) were comparable between the non-treated group and all treated groups. Lower doses (200, 500 mg/kg) of PBA and Nano<sup>PBA</sup> were well tolerated. However, higher doses of PBA (1000 mg/kg), Nano<sup>PBA</sup> ( $m = 30$ ) (1000 mg/kg), and Nano<sup>PBA</sup> ( $m = 49$ )

(1000 mg/kg)-treated groups resulted in lower liver weight compared to the healthy group (Figure 7f).

Two weeks post-administration, no significant differences were observed in RBCs (Figure 8a), WBCs (Figure 8b), hemoglobin (Figure 8c), and platelets (Figure 8d) between all PBA, Nano<sup>PBA</sup>-treated, and non-treated healthy groups. The plasma levels of liver damage markers, ALT and AST, were measured, and none of the PBA-treated groups showed significant elevation (Figure 8e,f). Lower doses of Nano<sup>PBA</sup> (100–500 mg/kg) were well tolerated without liver damage; however, the higher dose (1000 mg/kg) led to elevated levels of ALT. Interestingly, no significant changes in AST levels, another liver marker, were observed across any Nano<sup>PBA</sup> groups, indicating that the chosen doses were tolerable. Except for the high dose of PBA (81,000 mg/kg) and Nano<sup>PBA</sup> ( $m = 49$ ) (1000 mg/kg), all other groups showed comparable levels of kidney damage markers, BUN and CRE to the untreated group (Figure 8g,h). Furthermore, neither PBA nor Nano<sup>PBA</sup>-treated groups showed significant changes in the plasma levels of general markers ALB (Figure 8i), CPK (Figure 8j) and LDH (Figure 8k) compared to the non-treated control. These results indicate that the oral administration of Nano<sup>PBA</sup> (200–500 mg – PBA/kg – BW) did not exert any adverse effects as assessed by plasma organ damage markers, hematological parameters, and organ weight, which implies the suitability of the selected therapeutic dose.

## 4. Discussion

PBA is an FDA-approved drug used for the treatment of urea cycle disorders. Additionally, it has shown

of precursor and fragment ions. (b) Calibration curve of various authentic concentrations of authentic PBA and (c) mass spectra in PBS. (d)–(f) Mass spectrum of liberated PBA from Nano<sup>PBA</sup> for each unit of polymer at predetermined time. (g) The PBA release rate of Nano<sup>PBA</sup> in PBS, (h) total liberation of PBA, and (i) the area under the curve (AUC). (j) The PBA release rate of Nano<sup>PBA</sup> under SIF, (k) total liberation of PBA, and (l) AUC. (m) The PBA release rate of Nano<sup>PBA</sup> under SCF, (n) total liberation of PBA, and (o) AUC. The data are presented as the means  $\pm$  S.E.M; \*\*\* $p < 0.0002$ , \*\*\*\* $p < 0.0001$ , Tukey's multiple comparisons test.

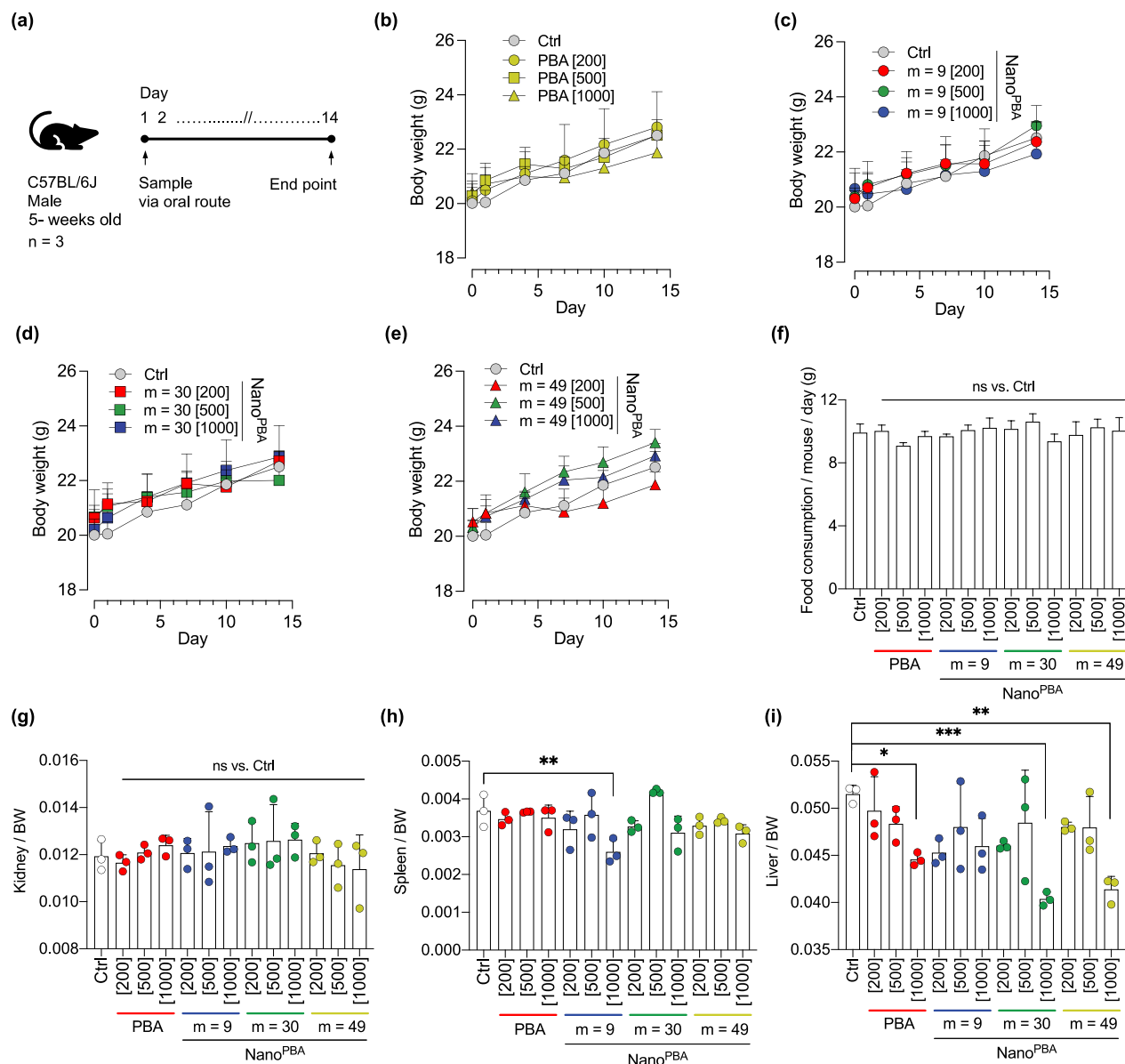


**Figure 7.** Body weight and organ weight of *in vivo* toxicity study. In this study, the mice (C57BL/6, male, 5 week) were divided into following 13 groups ( $n = 3$ ): healthy (water), PBA (100, 200, 500 mg/kg BW), Nano<sup>PBA</sup> for each unit of PBA (100, 200, 500 mg-PBA/kg BW). Sample solutions were administered orally once on the first day and observed till 2 weeks (a). Body weight of PBA group (b), Nano<sup>PBA</sup>  $m = 9$  group (c), Nano<sup>PBA</sup>  $m = 30$  group (d), Nano<sup>PBA</sup>  $m = 49$  group (e), and food consumption (f). Organ/body weight (BW) (g-i) at the experimental end point. The data are presented as the means  $\pm$  S.E.M; \* $p < 0.05$ , \*\* $p < 0.005$ , \*\*\* $p < 0.0005$ , Dunnett's multiple comparisons test.

efficacy in the managing cancer and neurodegenerative diseases, including Alzheimer's disease [11–13]. It functions as a histone deacetylase (HDAC) inhibitor, thereby modifying gene expression and inducing apoptosis [11–13]. PBA has been demonstrated to reduce ER stress by facilitating the refolding of misfolded proteins [11–13]. ER stress arises when the quantity of protein entering the ER surpasses its capacity to process them, frequently due to misfolding or low calcium levels. In response, cells activate the UPR, which entails a reduction in protein production, the degradation of misfolded proteins, and simultaneously increasing chaperones to facilitate proper folding. In the event that the stress is not effectively addressed, the UPR may result in apoptosis. In the context of cancer,

ER stress supports survival pathways such as angiogenesis and chemoresistance [2]. Consequently, reducing ER stress can induce cancer cell death.

Therapeutic utilization of PBA is limited due to its poor bioavailability which necessitates frequent dosing, resulting in adverse effects [10,16,17]. To address these pharmacokinetic limitations, a nanoparticle-based prodrug, Nano<sup>PBA</sup>, has been developed using MeO-PEG-*b*-P(VPBA) amphiphilic block copolymers (Figure 1 and 2) [18–21]. This design enables controlled, enzyme-responsive drug release, enhancing PBA's stability, safety, and pharmacokinetics [18–20].

The synthesis of PEG-*b*-P(VPBA) with different hydrophobic segments ( $m = 9, 30, 49$ ) was successfully achieved, as confirmed by <sup>1</sup>H-NMR and GPC



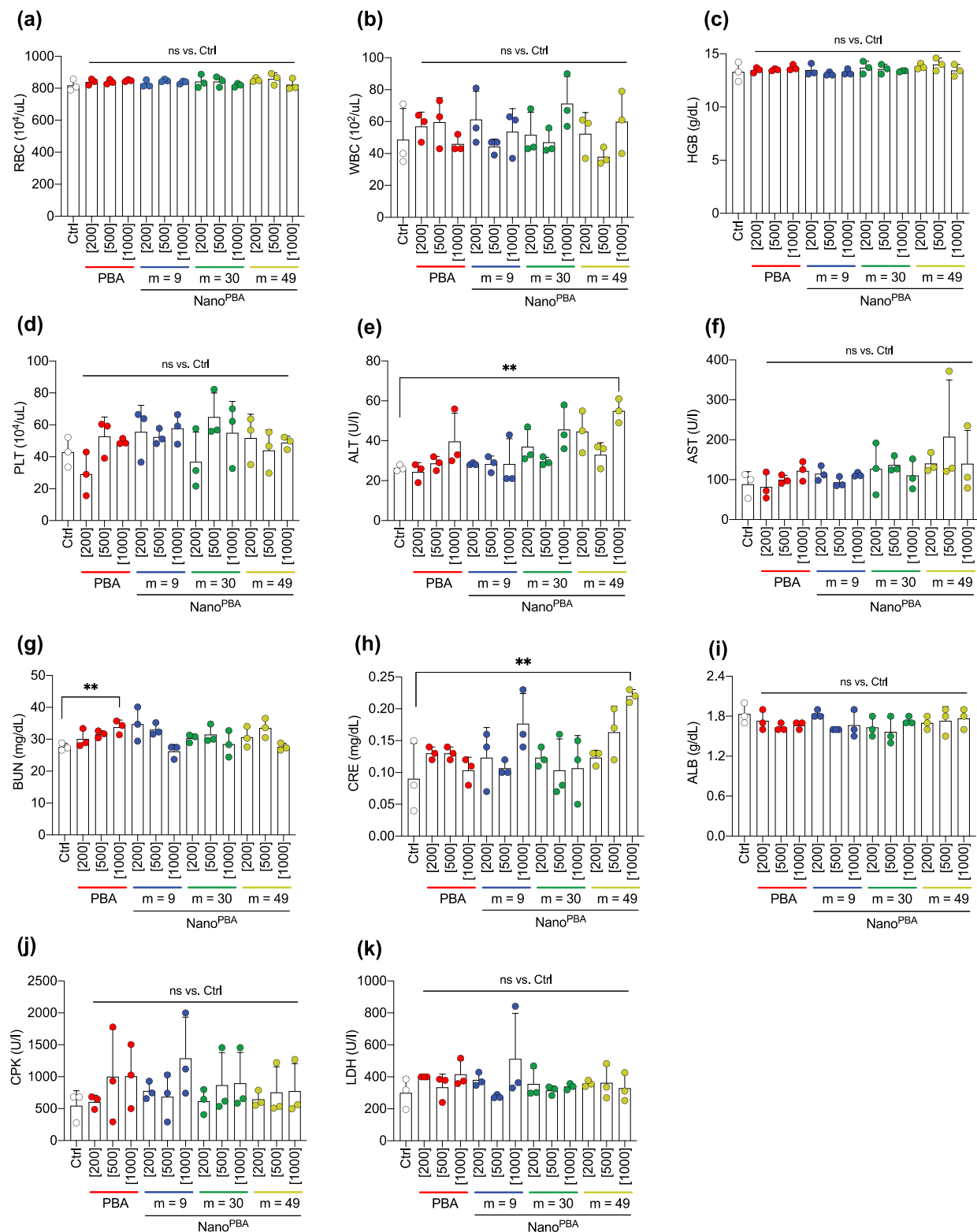


**Figure 8.** Analysis of hematology and plasma chemistry of *in vivo* toxicity study (Figure 7). A complete blood count measurement at the experimental endpoint; (a) RBC, (b) WBC, (c) HGB, and (d) PLT. Plasma organ damage markers at the experimental endpoint; (e) ALT, (f) AST, (g) BUN, (h) CRE, (i) ALB, (j) CPK, and (k) LDH. The data are presented as the means  $\pm$  S.E.M.; \*\* $p < 0.005$ , Bonferroni's multiple comparisons test.

(Figure 3). Nano<sup>PBA</sup> was prepared by self-assembly of amphiphilic PEG-*b*-P(VPBA) block copolymers in water. The hydrodynamic diameter (38–50 nm), with a PDI below 0.2, and the autocorrelation curve showing minimal fluctuations at room temperature indicates uniform micelle size (Figure 4a–c). The PEG shell of Nano<sup>PBA</sup> improves stability and biocompatibility by avoiding the formation of large aggregates and interactions with proteins [18–21,24]. The average Nano<sup>PBA</sup> size (38–50 nm) is ideal for avoiding rapid clearance (<5.5 nm) and phagocytic system activation (>100 nm) when administered systematically. This size also allows for longer intestinal retention when administered orally, improving micelle bioavailability [24,25]. Unlike conventional drug delivery systems, which physically entrap drugs in their core, the covalent conjugation of PBA to the polymer backbone prevents rapid leakage *in vivo*, minimizing potential side effects [18–21,23].

In this study, we evaluated the stability of Nano<sup>PBA</sup> for suitability for oral administration. The stability of the prepared Nano<sup>PBA</sup> was investigated under various pH conditions, ionic strength, simulated digestive fluids, and polymer concentrations (Figure 4d–o). We confirmed that regardless of the chain length of the hydrophobic segment (P(VPBA)) and micelle size, Nano<sup>PBA</sup> was stable in acidic and neutral conditions (pH 1–9), and collapsed under strong alkaline conditions (pH 9–13), indicating that all micelles would possibly maintain structural integrity under low pH condition of gastrointestinal (GI) tract. Stability studies under simulated digestive fluids showed that the micelle size shifted to larger diameter range in a longer time imply that the disintegration gradually occur by enzymatic and ionic activity in the intestine, and aggregation have formed. In the CMC evaluation, Nano<sup>PBA</sup> ( $m = 9$ ) showed the highest CMC (62.5 mg/L), followed by  $m = 30$  (5.9 mg/L) and  $m = 49$  (1.1 mg/L). Results indicate that an increase in the number of hydrophobic units in PEG-*b*-P(VPBA) leads to an increase in the hydrophobic interaction of the micelle core, resulting in the formation of stable micelles. Nano<sup>PBA</sup> nanostructure remains intact for a longer duration in diluted bodily fluids due to the thermodynamically governed equilibrium between micelle formation and disintegration, which contributes to its structural stability. Under digestive conditions, the micelles gradually collapse, exposing the ester moieties on the outer surface and making them more accessible [25,26,30]. These properties are promising for the prolongation of Nano<sup>PBA</sup> retention in gastric and intestinal fluids.

Previous research has shown that polymeric micelle with PEGylated shell would accumulate in the intestinal mucosa in a size-dependent manner, with smaller size retaining in the gastrointestinal tract for a long period of time after oral administration. Furthermore, PEG

chains of the micelle may lead to adhesion of micelles due to interdiffusion of mucus network and polymer entanglement with mucin composed of glycoprotein, increasing their intestinal residence time [24–26,30]. It is anticipated that with an increase in the intestinal residence time, the micelle will gradually collapse because of the super diluted conditions lower than the CMC, resulting in the exposure of ester moieties outside the micelle. This will lead to an increase in the attack of the intestinal enzyme against these moieties, thereby liberating the LMW drug for an extended period of time. To substantiate our hypothesis, an *in vitro* PBA release profile was obtained (Figure 5). In the absence of esterase, no PBA was detected. Conversely, when Nano<sup>PBA</sup> was added to the esterase solution, a gradual release of PBA was observed over time. The release rate decreased as the number of hydrophobic units increased, supporting the hypothesis that longer hydrophobic chains lead to more stable micelles and slower drug release. In addition, the release rate increased under digestive conditions such as SIF and SCF. These observations suggest that Nano<sup>PBA</sup>, composed of a polymer with a greater number of hydrophobic units forming more stable micelles, takes longer to disintegrate due to interactions with esterase. In contrast, polymers with shorter hydrophobic units exhibit faster disintegration and accelerated PBA release through hydrolysis. Furthermore, stability studies showed that micelles disintegrate more slowly under SIF and SCF conditions, indicating that the presence of enzymes and ionic activity in the intestine promotes micelle degradation. This allows enzymes to access and briefly interact with the hydrophobic segments, resulting in an increased release rate. These results highlight the importance of analyzing polymers with varying degrees of polymerization, as these differences significantly affect their *in vivo* characteristics. This indicates that the disintegration of micelles is kinetically controlled rather than thermodynamically, and that after exposing the hydrophobic segment outside, they undergo hydrolysis through an enzymatic reaction.

To validate PBA liberation under *in vivo* conditions, we previously confirmed the pharmacokinetic parameters using radiolabeled Nano<sup>PBA</sup>. <sup>125</sup>Iodine (<sup>125</sup>I) was installed to phenyl moiety of Nano<sup>PBA</sup> and orally administered to C57BL/6J mice [18]. After 24 h of oral administration, a certain level of radioactive signals was observed from blood, liver, kidney, spleen, lungs, and heart, indicating a successful hydrolysis of ester linkage of <sup>125</sup>I-Nano<sup>PBA</sup> in the GI tract. We also confirmed that only liberated PBA was internalized into the bloodstream, while the rest of the polymer remains in the GI tract [18]. This pharmacokinetic characteristic, i.e. the lack of nanoparticle internalization and liberated short-chain fatty acids internalizing the bloodstream, is critical to avoid potential adverse effects or burdens on the clearance organs.

Additionally, other than the oral route, we also confirmed the improvement of the pharmacokinetic profile of PBA using parental intraperitoneal administration [20]. Interperitoneally administered  $^{125}\text{I}$ -Nano<sup>PBA</sup> to tumor-bearing mice (B16 melanoma) showed high radioactivity signals in the blood and tumor until 48 h, whereas LMW  $^{125}\text{I}$  was cleared within 24 h of administration [20]. Our previous pharmacokinetic evaluations confirm that the polymer design may achieve improved bioavailability of PBA, which subsequently leads to higher efficacy in the disease models. In the future, comparative PK studies of Nano<sup>PBA</sup> should be conducted using various dosages and different routes of administration, including oral, intraperitoneal, intravenous, and subcutaneous methods, in both healthy and diseased mouse models. It will be more interesting to compare with those of low-molecular-weight counterparts.

One of the most crucial elements in the advancement of novel biomaterials is their biocompatibility. If the material to be utilized within the human body is not biocompatible, the immune system may mount an immune response, potentially leading to the impairment of biological function. In the present study, the cytotoxicity of Nano<sup>PBA</sup> was evaluated using BAEC, RAW-264.T, and RGM-1. The viability results show the Nano<sup>PBA</sup>-treated group did not decrease in cell viability relative to the PBA group at a high concentration range (Figure 6). The primary rationale for this phenomenon might be attributed to the fact that the surface of Nano<sup>PBA</sup> is coated with densely packed PEG tethered chains, which effectively inhibits the uptake capacity of normal cells and thus prevents rejection when in contact with cells [30–35]. Our data suggest that the Nano<sup>PBA</sup> prepared in this study displays minimal cytotoxicity *in vitro* compared with LMW PBA. We further investigated the toxicological changes upon Nano<sup>PBA</sup> and PBA administration (Figures 7 and 8). The results indicate that the oral administration of Nano<sup>PBA</sup> (200–500 mg – PBA/kg – BW) did not exert any adverse effects as assessed by plasma organ damage markers, hematological parameters, and organ weight, while in administration at higher concentration (1000 mg – PBA/kg – BW) showed effects on organs, which implies the suitability of the selected therapeutic dose to be less than 500 mg – PBA/kg – BW [18–21]. In the context of nanoparticle-based applications, the PBA concentration does not exhibit a rapid increase in the initial stages, thereby reducing the likelihood of PBA-induced toxicity. Conversely, the administration of micelles at remarkably elevated concentrations has the potential to induce kidney toxicity, a phenomenon that may be attributable to disruptions in the bile acid cycle, including bile acid adsorption within the digestive tract.

In conclusion, Nano<sup>PBA</sup> represents a promising advancement in the field of prodrug delivery systems, particularly for enhancing the pharmacokinetics and therapeutic efficacy of PBA, and differs from conventional methods that simply involve physically encapsulating drugs into nanoparticles. By employing a polymeric nanoparticle design that ensures controlled, enzyme-responsive drug release, Nano<sup>PBA</sup> effectively addresses the significant challenges associated with traditional delivery methods, such as rapid clearance and potential cytotoxicity. The capacity to modify the release rate through alterations to the hydrophobic units represents a further enhancement of its potential for tailored therapeutic applications. The favorable biocompatibility and stability of Nano<sup>PBA</sup>, demonstrated in both *in vitro* and *in vivo* studies, highlight its suitability for clinical use, particularly in targeting diseases where sustained drug release and minimal side effects are essential.

## Disclosure statement

No potential conflict of interest was reported by the author(s).

## Funding

This research was funded by the Ministry of Education, Culture, Sports, Science and Technology (MEXT), Japan, grant number [19H05458].

## Author contributions

Conceptualization, Y.N. and B.S.; methodology, K.M., B. S. and H.M.; validation, K.M and B.S.; formal analysis, K. M and B.S.; investigation, K.M, B.S. and Y.N.; data curation, K.M and B.S.; writing – original draft preparation, K.M and B.S; writing – review and editing, K.M, B.S., and Y.N.; visualization, K.M and B.S.; supervision, Y.N.; project administration, B.S.; funding acquisition, Y.N. All authors have read and agreed to the published version of the manuscript.

## References

- [1] Koksai AR, Verne GN, Zhou Q. Endoplasmic reticulum stress in biological processing and disease. *J Investig Med*. 2021;69(2):309–315. doi: [10.1136/jim-2020-001570](https://doi.org/10.1136/jim-2020-001570)
- [2] Hotamisligil GS. Endoplasmic reticulum stress and the inflammatory basis of metabolic disease. *Cell*. 2010;140(6):900–917. doi: [10.1016/j.cell.2010.02.034](https://doi.org/10.1016/j.cell.2010.02.034)
- [3] Hetz C, Chevet E, Harding HP. Targeting the unfolded protein response in disease. *Nat Rev Drug Discov*. 2013;12(9):703–719. doi: [10.1038/nrd3976](https://doi.org/10.1038/nrd3976)
- [4] Khaled J, Kopsida M, Lennernäs H, et al. Drug resistance and endoplasmic reticulum stress in hepatocellular carcinoma. *Cells*. 2022;11(4):632. doi: [10.3390/cells11040632](https://doi.org/10.3390/cells11040632)
- [5] Karagöz GE, Acosta-Alvear D, Walter P. The unfolded protein response: detecting and responding

- to fluctuations in the protein-folding capacity of the endoplasmic reticulum. *Cold Spring Harb Perspect Biol.* **2019**;11(9):a033886. doi: [10.1101/cshperspect.a033886](https://doi.org/10.1101/cshperspect.a033886)
- [6] Scriven P, Coulson S, Haines R, et al. Activation and clinical significance of the unfolded protein response in breast cancer. *Br J Cancer.* **2009**;101:1692–1698. doi: [10.1038/sj.bjc.6605365](https://doi.org/10.1038/sj.bjc.6605365)
  - [7] Nagelkerke A, Bussink J, van der Kogel AJ, et al. The PERK/ATF4/LAMP3-arm of the unfolded protein response affects radioresistance by interfering with the DNA damage response. *Radiother Oncol.* **2013**;108(3):415–421. doi: [10.1016/j.radonc.2013.06.037](https://doi.org/10.1016/j.radonc.2013.06.037)
  - [8] Gomez BP, Riggins RB, Shajahan AN, et al. Human X-box binding protein-1 confers both estrogen independence and antiestrogen resistance in breast cancer cell lines. *FASEB J.* **2007**;21:4013–4027. doi: [10.1096/fj.06-7990com](https://doi.org/10.1096/fj.06-7990com)
  - [9] Papp E, Csermely P. Chemical chaperones: mechanisms of action and potential use. *Mol Chaperones Heal Dis Handb Exp Pharmacol.* **2006**;172:405–416.
  - [10] FDA-Approved Drugs Database on U.S.A. Food and drug administration website. [cited Dec 10] Available from: <https://www.accessdata.fda.gov/scripts/cder/daf/index.cfm?event=overview.process&ApplNo=020572>
  - [11] Qian K, Sun L, Zhou G, et al. Sodium phenylbutyrate inhibits tumor growth and the epithelial-mesenchymal transition of oral squamous cell carcinoma in vitro and in vivo. *Cancer Biother Radiopharm.* **2018**;33(4):139–145. doi: [10.1089/cbr.2017.2418](https://doi.org/10.1089/cbr.2017.2418)
  - [12] Kolb PS, Ayaub EA, Zhou W, et al. The therapeutic effects of 4-phenylbutyric acid in maintaining proteostasis. *Int J Biochem Cell Biol.* **2015**;61:45–52. doi: [10.1016/j.biocel.2015.01.015](https://doi.org/10.1016/j.biocel.2015.01.015)
  - [13] Cuadrado-Tejedor M, Ricobaraza AL, Torrijo R, et al. Phenylbutyrate is a multifaceted drug that exerts neuroprotective effects and reverses the Alzheimer's disease-like phenotype of a commonly used mouse model. *Curr Pharm Des.* **2013**;19(28):5076–5084. doi: [10.2174/1381612811319280006](https://doi.org/10.2174/1381612811319280006)
  - [14] Cuadrado-Tejedor M, García-Osta A, Ricobaraza A, et al. Defining the mechanism of action of 4-phenylbutyrate to develop a small-molecule-based therapy for Alzheimer's disease. *Curr Med Chem.* **2011**;18(36):5545–5553. doi: [10.2174/092986711798347315](https://doi.org/10.2174/092986711798347315)
  - [15] Li LZ, Deng HX, Lou WZ, et al. Growth inhibitory effect of 4-phenyl butyric acid on human gastric cancer cells is associated with cell cycle arrest. *World J Gastroenterol.* **2012**;18(1):79–83. doi: [10.3748/wjg.v18.i1.79](https://doi.org/10.3748/wjg.v18.i1.79)
  - [16] Nakano S, Osaka S, Sabu Y, et al. Effect of food on the pharmacokinetics and therapeutic efficacy of 4-phenylbutyrate in progressive familial intrahepatic cholestasis. *Sci Rep.* **2019**;9:17075. doi: [10.1038/s41598-019-53628-x](https://doi.org/10.1038/s41598-019-53628-x)
  - [17] Phenylbutyric acid: uses, interactions, mechanism of actions. [cited Dec 7]. Available from: <https://go.drugbank.com/drugs/DB06819>
  - [18] Shashni B, Tajika Y, Nagasaki Y, et al. Design of enzyme-responsive short-chain fatty acid-based self-assembling drug for alleviation of type 2 diabetes mellitus. *Biomaterials.* **2021**;275:120877. doi: [10.1016/j.biomaterials.2021.120877](https://doi.org/10.1016/j.biomaterials.2021.120877)
  - [19] Shashni B, Tajika Y, Ikeda Y, et al. Self-assembling polymer-based short chain fatty acid prodrugs ameliorate non-alcoholic steatohepatitis and liver fibrosis. *Biomaterials.* **2023**;295:122047. doi: [10.1016/j.biomaterials.2023.122047](https://doi.org/10.1016/j.biomaterials.2023.122047)
  - [20] Shashni B, Nagasaki Y. Self-assembling butyric acid prodrug acts as a sensitizer for cancer radiotherapy. *Nano Today.* **2024**;54:102103. doi: [10.1016/j.nantod.2023.102103](https://doi.org/10.1016/j.nantod.2023.102103)
  - [21] Shashni B, Nagasaki Y. Short-chain fatty acid-releasing nano-prodrugs for attenuating growth and metastasis of melanoma. *Acta Biomater.* **2023**;159:226–236. doi: [10.1016/j.actbio.2023.01.054](https://doi.org/10.1016/j.actbio.2023.01.054)
  - [22] Taninaka A, Kurokawa H, Kamiyanagi M, et al. pol-philiprotein-induced autophagy mechanism with high performance in photodynamic therapy. *Commun Biol.* **2023**;6(1):1212. doi: [10.1038/s42003-023-05598-0](https://doi.org/10.1038/s42003-023-05598-0)
  - [23] Vong L, Tomita T, Yoshitomi T, et al. An orally administered redox nanoparticle that accumulates in the colonic mucosa and reduces colitis in mice. *Gastroenterology.* **2012**;143(4):1027–1036.e3. doi: [10.1053/j.gastro.2012.06.043](https://doi.org/10.1053/j.gastro.2012.06.043)
  - [24] Wang YY, Lai SK, Suk JS, et al. Addressing the PEG mucoadhesivity paradox to engineer nanoparticles that “slip” through the human mucus barrier. *Angew Chem Int Ed Engl.* **2008**;47(50):9726–9729. doi: [10.1002/anie.200803526](https://doi.org/10.1002/anie.200803526)
  - [25] Lai SK, Wang YY, Wirtz D, et al. Micro- and macro-rheology of mucus. *Adv Drug Deliv Rev.* **2009**;61(2):86–100. doi: [10.1016/j.addr.2008.09.012](https://doi.org/10.1016/j.addr.2008.09.012)
  - [26] Shashni B, Nishikawa Y, Nagasaki Y. Management of tumor growth and angiogenesis in triple-negative breast cancer by using redox nanoparticles. *Biomaterials.* **2021**;269:120645. doi: [10.1016/j.biomaterials.2020.120645](https://doi.org/10.1016/j.biomaterials.2020.120645)
  - [27] Bosch M, Schlaf M. Synthesis of allyl and alkyl vinyl ethers using an in situ prepared air-stable palladium catalyst. Efficient transfer vinylation of primary, secondary, and tertiary alcohols. *J Org Chem.* **2003**;68(13):5225–5227. doi: [10.1021/jo034376h](https://doi.org/10.1021/jo034376h)
  - [28] Basu Ray G, Chakraborty I, Moulik SP. Pyrene absorption can be a convenient method for probing critical micellar concentration (cmc) and indexing micellar polarity. *J Colloid Interface Sci.* **2006**;294(1):248–254. doi: [10.1016/j.jcis.2005.07.006](https://doi.org/10.1016/j.jcis.2005.07.006)
  - [29] Marahatta A, Bhandary B, Lee M-R, et al. Determination of phenylbutyric acid and its metabolite phenylacetic acid in different tissues of mouse by liquid chromatography with tandem mass spectrometry and its application in drug tissue distribution. *J Chromatogr B.* **2012**;903:118–125. doi: [10.1016/j.jchromb.2012.07.004](https://doi.org/10.1016/j.jchromb.2012.07.004)
  - [30] Sha S, Vong LB, Chonpathompikunlert P, et al. Suppression of NSAID-induced small intestinal inflammation by orally administered redox nanoparticles. *Biomaterials.* **2013**;34(33):8393–8400. doi: [10.1016/j.biomaterials.2013.06.032](https://doi.org/10.1016/j.biomaterials.2013.06.032)
  - [31] Shashni B, Tamaoki J, Kobayashi M, et al. Design of novel self-assembling antioxidant nanomedicine to ameliorate oxidative stress in zebrafish embryos. *Acta Biomater.* **2023**;159:367–381. doi: [10.1016/j.actbio.2023.01.012](https://doi.org/10.1016/j.actbio.2023.01.012)



- [32] Shashni B, Nagasaki Y. Nitroxide radical-containing nanoparticles attenuate tumorigenic potential of triple negative breast cancer. *Biomaterials*. 2018;178:48–62. doi: [10.1016/j.biomaterials.2018.05.042](https://doi.org/10.1016/j.biomaterials.2018.05.042)
- [33] Shashni B, Horiguchi Y, Kurosu K, et al. Application of surface enhanced Raman spectroscopy as a diagnostic system for hypersialylated metastatic cancers. *Biomaterials*. 2017;134:143–153. doi: [10.1016/j.biomaterials.2017.04.038](https://doi.org/10.1016/j.biomaterials.2017.04.038)
- [34] Qin C, Wang H, Cui H, et al. Synthetic genomic nanomedicine with triple-responsiveness for systemic anti-tumor therapy. *J Colloid Interface Sci*. 2024;672:350–362. doi: [10.1016/j.jcis.2024.06.010](https://doi.org/10.1016/j.jcis.2024.06.010)
- [35] Shashni B, Alshwimi A, Minami K, et al. Nitroxide radical-containing nanoparticles as potential candidates for overcoming drug resistance in epidermoid cancers. *Polymer*. 2017;116:429–438. Available from: <https://www.sciencedirect.com/science/article/pii/S0032386117301763>